J. Min. Metall. Sect. B-Metall. 49 (1) B (2013) 83 - 89

Journal of Mining and Metallurgy, Section B: Metallurgy

THE INFLUENCE OF Si AND V ON THE KINETICS OF PHASE TRANSFORMATION AND MICROSTRUCTURE OF RAPIDLY SOLIDIFIED Al-Fe-Zr ALLOYS

B. Karpe[a,*], B. Kosec[a], A. Nagode[a], M. Bizjak[a]

[a] *University of Ljubljana, Faculty of Natural Science and Engineering, Ljubljana, Slovenia*

(Received 14 February 2013; accepted 27 June 2013)

Abstract

The influence of Si and V on the precipitation kinetics of the rapidly solidified (RS) Al-Fe-Zr alloys is presented. Precipitation kinetics and microstructural development of RS Al-Fe-Zr alloys with Si or V addition have been investigated by the combination of four point electrical resistance measurement, optical microscopy, transmition electron microscopy (TEM) and scanning electron microscopy (SEM). For verification of the electrical resistivity measurement results differential scanning calorimetry (DSC) and differential thermal analysis (DTA) was also applied. Rapidly solidified samples, in the form of thin ribbons, were prepared with the single roll melt spun technique. For determination of the distinctive temperatures at which microstructural transformations occur in-situ electrical resistivity measurement during heating of the ribbons with various constant heating rates has been used. It was found that microstructure decomposition depends on heating rate and shifts to higher temperatures with increasing heating rate. After heating above the distinctive transition temperatures, heating was stopped and microstructure of the samples examined by electron microscopy.

Keywords: *Rapidly solidification; Al-Fe-Zr alloys; Microstructure transformation; Precipitation; Electrical resistance measurement.*

1. Introduction

The greatest hardening effect in aluminum alloys can be obtained by precipitation of extremely small, uniformly and densely dispersed intermetalic particles in the aluminum matrix. To achieve such a final state of microstructure, solution annealing with subsequent precipitation heat treatment has to be used. Unfortunately, conventional procedures are suitable only for alloys containing alloying elements with a substantial solid solubility at solution annealing temperature. For synthesis of precipitation hardened aluminum alloys containing elements with poor solid solubility new approaches have to be applied [1].

With the development of rapid solidification and powder metallurgy (RS/PM), syntheses of such alloys became possible. Due to extremely high solidification rate, rapid solidification processes enable higher solubility of alloying elements in the metal matrix, fine grain microstructure and formation of finely dispersed intermetalic particles. Usually the material produced by rapid solidification processes is in the unsuitable form (ribbons, flakes, powder …) and has to be consolidated with the proper powder metallurgy process which can preserve the benefits of rapid solidification [2].

Aluminum alloys with good mechanical properties at elevated temperatures usually contain slow-diffusivity transition metals or lanthanides [3, 4]. Most of the successful developed alloys contain iron. However, in binary RS/PM Al-Fe alloys, sharp fall in strength occurs during heating above 300-350°C. The main reason for this is a coarsening of the structure due to coagulation of fine intermetalic particles and transition of metastable phases (Al_6Fe, Al_mFe) to stable phase Al_3Fe [5, 6]. Further development of the structure stabilization was based on three following principles: adding elements (Mo) which inhibit iron diffusion in aluminum; elements (Ce, Si, V …) which enters in Al_mFe phases and forms complex AlFeX phases stable at higher temperatures or elements (Zr) which form an iron-free phases by precipitation from supersaturated a_{Al} solid solution [3, 7]. The aim of this work was to examine the effect of Si and V addition on the microstructure of rapidly solidified Al-Fe-Zr alloy and to investigate the sequence and kinetics of precipitation phenomena from supersaturated a_{Al} solid solution with the electrical resistivity measurements.

2. Experimental

Rapidly solidified ribbons of Al-Fe-Zr (AZ), Al-

* *Corresponding author: blaz.karpe@omm.ntf.uni-lj.si*

DOI:10.2298/JMMB130214023K

Fe-Zr-Si (AS) and Al-Fe-Zr-V (AV) alloys were manufactured with the single roll melt spinning apparatus. The cast precursors were inserted into the graphite crucible and inductively melted in argon atmosphere at the absolute pressure of 420 mbar and sprayed under the overpressure through the nozzle of the diameter of 1,0 mm into the rotating copper wheel. Average thickness of analyzed ribbons was approximately 70 mm. The chemical composition of the ribbons is shown in Table 1.

Table 1. *Alloys chemical composition*

Alloy code	Chemical composition /wt.%				Σ(Alloying elements) /wt. %
	Fe	Zr	V	Si	
AZ	7.00	1.01	0.00	0.00	8.01
AS	7.70	0.97	0.00	2.30	10.95
AV	5.86	0.95	1.20	0.00	8.11

Kinetics and the sequence of the microstructural transformations in the RS ribbons were investigated by the in-situ measurements of the electrical resistance during heating with the constant heating rate in the tube-furnace under argon protective atmosphere. The four-point D.C. electrical resistivity measurement method with tungsten contacts and platinum wires was applied for the measurement of the electrical resistance. DSC (Netzsch DSC 200) and DTA (Type 701-Bahr Thermo-analyse) methods were also used for following the microstructural transformation during constant heating rate on similar samples. Microstructure was examined before and after heat treatment. After heating up to distinctive temperatures (T_{mx}), determined by electrical resistivity measurements, heating was stopped and microstructure of the samples examined by electron microscopy. Samples for SEM observation were prepared according to the classical metallographic procedure and etched with Keller's reagent. Thin foils for TEM observation were prepared by grinding the ribbons to approximately 40 mm, cutting the 3 mm diameter disks and ion thinned with Gatan PIPS M.691.

3. Results and discussion

3.1 Microstructure of rapidly solidified ribbons

All previous studies of the rapidly solidified binary Al-Fe [4, 8] and multi-component Al-Fe-X [9] alloys reported two distinctive morphologies of the solidification. The zone of the extremely refined microstructure designated as zone A, and zone with coarser microstructure containing larger intermetallic particles designated as zone B [10]. Studies of the formation of zones A and B suggest that a high degree of the melt undercooling at the solidifying interface is essential to the production of zone A, and that thermal recalescence during solidification reduces the effective undercooling of the remaining melt and results in the formation of the zone B. The microstructure of the examined rapidly solidified ribbons shows dual zone morphology of solidification [11]. Approximately 20 mm wide layer of nano-cell microstructure, which was in the contact with the chilling wheel, and a layer of micro-cell microstructure, which extends to the free surface of the ribbon (Fig.1). The transition between the zones is well visible. The proportion of the individual zone depends mainly on the ribbon thickness and physical contact between the spinning wheel and the melt. Thinner is the ribbon, larger is the extent of the nano-cell zone A, but only in the case of good physical contact. Entrapped gas at the contact surface, either from surrounding atmosphere or the melt itself, reduces the heat transfer considerably, and causing the extent of the zone B through entire ribbon thickness [12]. In the case of good physical contact and ribbon thickness thinner that approximately 15mm only zone A will be observed.

3.2 Electrical resistivity measurement

It has been shown that in-situ electrical resistivity measurements can be a very suitable and precise experimental method for following the microstructural changes and phase transformations in some metallic alloys [13, 14], especially for Al-based alloys in quenched state [15, 16]. The results of the electrical resistance measurements during heating

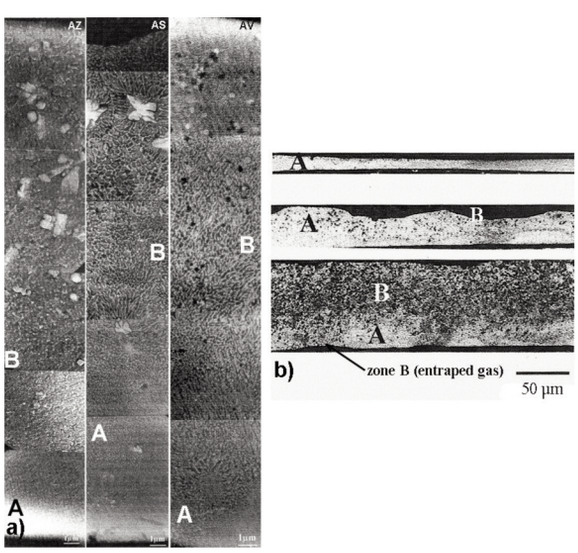

Figure 1. *a) Microstructure over a transverse cross section of rapidly solidified AZ, AS and AV alloy ribbons (thickness approx. 70mm), b) microstructure of AZ alloy at various ribbon thicknesses*

with constant heating rate are presented in Fig.2. At lower temperatures, Al-Fe-Zr-X alloys exhibit practically linear increase of electrical resistance with increasing temperature. At higher temperatures, the change of electrical resistivity becomes nonlinear. This can be seen more precisely on the electrical resistivity derivative curve ($^{dR}/_{dT}$). First nonlinear change of the electrical resistivity is detected in the temperature interval, with the maximum rate of electrical resistivity decrease at temperature T_{m1} (derivation minima). It is well known that any kind of crystal lattice distortion, caused by solute atoms, impurities, dislocations, etc., increases electrical resistivity of the metal. Therefore, nonlinear change of electrical resistivity must be related to the microstructural transformations in the material matrix. Because solute atoms are particularly effective scattering centers for electrons, major contribution to the initial electrical resistivity decrease is related to the precipitation of solute atoms from the saturated crystal lattice. Additionally, less intense electrical resistivity decrease was detected in the second temperature interval, with the maximum rate of the electrical resistivity decrease at temperature T_{m2} (Fig.2). It should be noted, that for all analyzed alloys temperature T_{m2} was practically equal (537±2°C at a constant heating rate 5K/min).

Figure 3 shows a comparison of the results obtained by DTA, DSC and electrical resistivity measurements during constant heating rate of 5 K/min for AS alloy. As can be seen, the temperature of the exothermal peak on DTA and DSC curves coincide well with the temperature of the first minima on the electrical resistivity derivation curve. The difference between T_{m1} and DSC and DTA exothermal peak temperature is only 1,5°C for AS and 0,8°C for AV alloy. On the contrary, DTA and DSC measurements didn't detect any heat generation at the temperature T_{m2} where the second electrical resistivity minima was recorded.

With increasing heating rate the overall electrical resistance temperature dependency remains equal, except that the beginning of microstructure decomposition is shifted to higher temperatures. These shifts are the result of shorter time available for the start of the reaction. Figure 4 shows electrical resistivity temperature dependencies, and its derivation curve as a function of heating rate for AV alloy. Measured values of the T_{m1} temperatures for the AZ, AS and AV alloys are presented in Table 2.

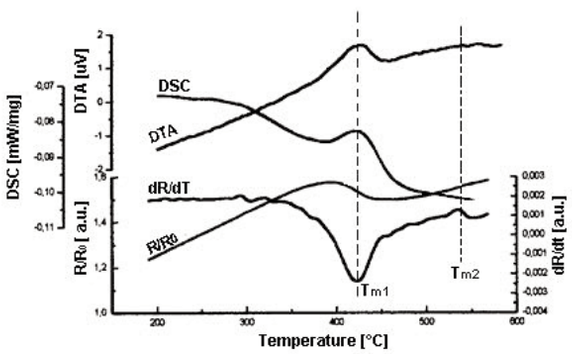

Figure 3. *Comparison between electrical resistance, DTA and DSC curves recorded at a constant heating rate of 5 K/min for AS alloy.*

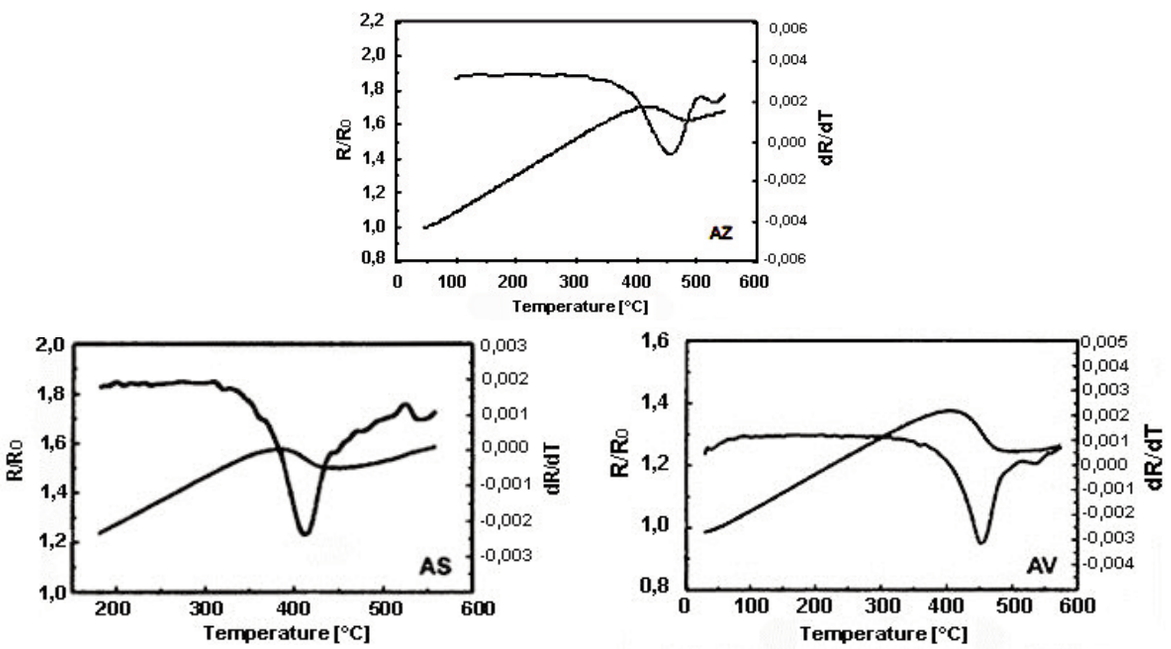

Figure 2. *Electrical resistivity and its temperature derivative for AZ, AS and AV alloy at a constant heating rate of 5K/min.*

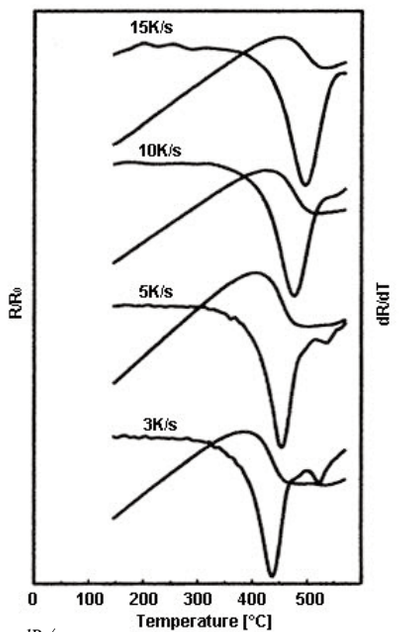

Figure 4. *$^{dR}/_{dT}$ curves as a function of heating rate for AV alloy.*

Table 2. *Temperatures of the electrical resistance minima (T_{m1}) on ($^{dR}/_{dT}$) curve*

Heating rate β (K/μιν)	T_{m1} (°C)		
	AZ	AS	AV
3	440	398	437
5	460	420	456
10	496	447	478
15	516	463	497

3.3 Microstructure and transformation sequence of the RS Al-Fe-Zr (AZ) alloy

Microstructure of rapidly solidified ribbon of the AZ alloy consists of two zones. A layer of supersaturated a_{Al} nano-cells fringed with fine net of metastable Al_mFe eutectic phases, and micro-cell layer, composed of supersaturated a_{Al} micro-cells with discontinuous eutectic net on cell boundaries. Regions of larger oval and beam like intermetalic particles surrounded by a_{Al} micro-cells can be seen towards the free surface of the ribbon. Microcell growth, perpendicular to the particle interface, indicates primary crystallization of larger particles. Oval particles were identified by electron diffraction as orthorhombic metastable Al_6Fe phase and beam shape particles as a monoclinic stable phase with stoichiometric composition corresponding to $Al_{13}Fe_4$ phase. Because an extensive homogeneity region of this phase, from 37,2 ± 0,2 to 41,1 ± 0,2 wt.% Fe (Griger et al. 1986, Lendvai et al. 1986), this phase can be described by different formulas: Al_7Fe_4, $Al_{13}Fe_4$, $Al_{19}Fe_6$ and Al_3Fe. By EDX analysis, zirconium was detected only in the interior of the cells.

Sequences of microstructural transformations in ribbon samples were detected by measurement of the electrical resistance during heating and analyzed by electron microscopy. Two deviations from linearity of the electrical resistance were detected during heating to 600°C. First one, in the temperature interval with the dR/dT minima at $T_{m1\text{-}AZ}$ (table 2), and second in the temperature interval with the dR/dT minima at $T_{m2\text{-}AZ}$ (Fig.2). At the beginning of the first temperature interval, up to 400°C, no significant changes in the microstructure were seen. Above temperature T_{m1} the cellular microstructure completely disintegrated (Fig.5).

Large amount of needle shaped particles of approximate 200 nm in length and 35 nm in diameter precipitated from the matrix (Fig 6a). By electron diffraction method, needle shaped particles were identified as a monoclinic $Al_{13}Fe_4$ stable phase. The presence of the globular Al_6Fe phase in the microstructure proves that microstructure transformation isn't finished. Zirconium was detected

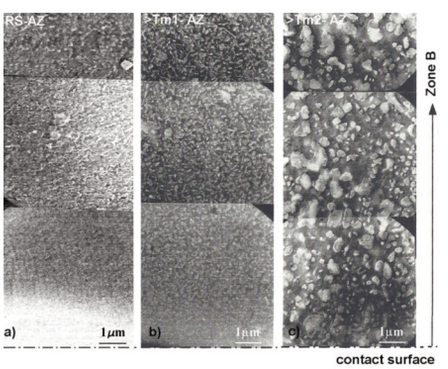

Figure 5. *Microstructure of AZ alloy (SEM), a) rapidly solidified, b) after heating up to T_{m1}, c) after heating up to T_{m2}*

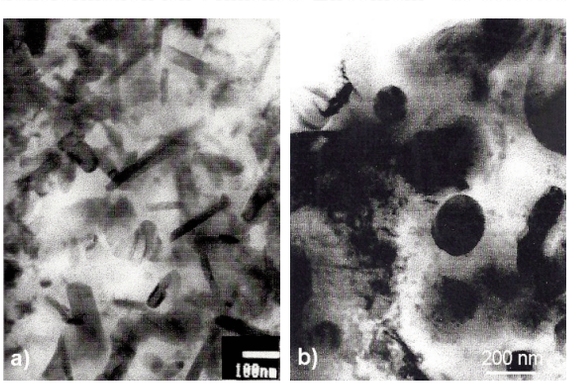

Figure 6. *Microstructure of AZ alloy (TEM), a) precipitation of needle shape $Al_{13}Fe_4$ particles during heating up to T_{m1}, b) precipitation of globular Al_3Zr particles during heating up to T_{m2}*

only in the a_{Al} solid solution. During the heating above $T_{m2\text{-}AZ}$ temperature, spheroidization of needle shaped particles and their growth into oval or globular particles occurred. No particles of Al_6Fe phase were found, indicating the complete transformation of metastable into stable iron phases above T_{m2} temperature. Besides in small globular particles identified as Al_3Zr phase, zirconium was also found in larger globular $Al_3Fe(Zr)$ phase particles (Fig.6b).

3.4 Microstructure and transformation sequence of the Al-Fe-Zr-Si (AS) alloy

As in the case of AZ alloy, microstructure of AS rapidly solidified ribbons also consists of nano and micro-cell layers (Fig.7). By electron diffraction we were unable to identify the eutectic phases in the intercellular region. The EDX analysis showed that intercellular region is rich in aluminium, iron and silicon. The only conclusion we can give at this point is that intercellular region consists of complex Al-Fe-Si eutectic. Regions of larger $Al_xFe_ySi_z$ intermetalic particles, surrounded by a_{Al} micro-cells can be seen towards the free surface of the ribbon. Microcell growth perpendicular to the particle interface indicates primary crystallization of larger particles.

Sequence of microstructural transformation in the AS alloy during heating differ from those of the Al-Fe-Zr alloy. In the initial temperature interval, with the dR/dT minima at $T_{m1\text{-}AS}$, the cell microstructure was gradually transformed into randomly oriented $Al_xFe_ySi_z$ spherical particles in the a_{Al} matrix (Fig.8). Decomposition of the cell microstructure and the precipitation from the supersaturated a_{Al} solid solution directly into the spherical particles is attributed to the silicon influence. Zirconium was detected only in the a_{Al} solid solution. By heating up to $T_{m2\text{-}AS}$ temperature, metastable $Al_xFe_ySi_z$ phase transformed into stable Al_3FeSi phase. Zirconium precipitated in the form of globular, 20¸50 nm large particles identified as Al_3Zr phase (Fig. 9).

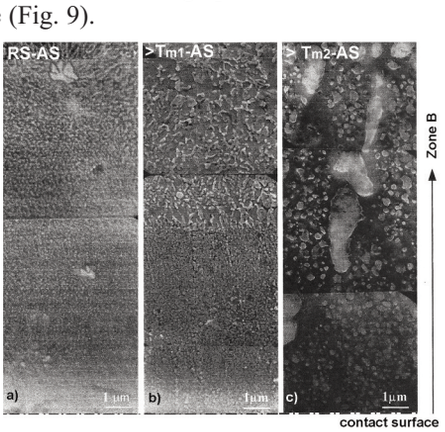

Figure 7. *Microstructure of AS alloy (SEM), a) rapidly solidified, b) after heating up to T_{m1}, c) after heating up to T_{m2}*

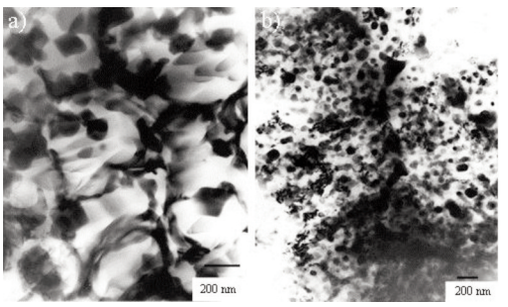

Figure 8. *a) Cell microstructure of the rapidly solidified AS alloy, b) precipitation of globular silicides during heating up to T_{m1}*

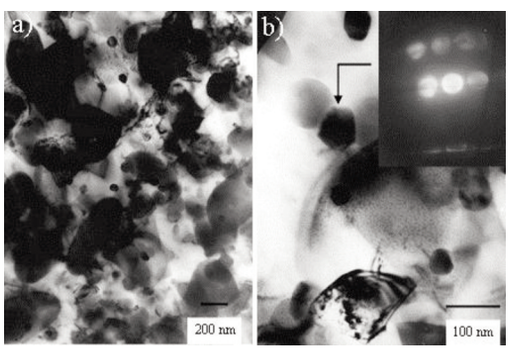

Figure 9. *a) Microstructure of the AS alloy after heating up to T_{m2}, b) globular Al_3Zr phase*

3.5 Microstructure and transformation sequence of the Al-Fe-Zr-V (AV) alloy

Microstructure of rapidly solidified ribbons of AV alloy also has the cell microstructure with metastable Al_mFe eutectic phases on the cell boundaries as in the case of RS AZ alloy (Fig.10). The major difference is the absence of larger primary crystallized particles in the zone B. Vanadium and zirconium were detected in the a_{Al} solid solution as in the fine globular particles. Amount of $Al_xFe(V, Zr)$ particles is small and increasing towards the free surface of the ribbon.

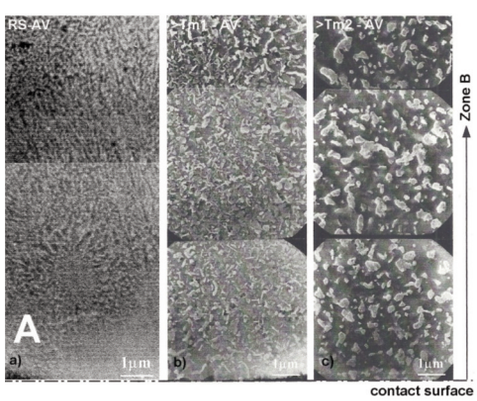

Figure 10. *Microstructure of AV alloy (SEM), a) rapidly solidified, b) after heating up to T_{m1}, c) after heating up to T_{m2}*

Table 3. *Microstructure of rapid solidified AZ, AS and AV alloys before and after heat treatment.*

Alloy type	Alloy microstructure		
	Rapidly solidified	After heating to T_{m1}	After heating to T_{m2}
Al-Fe-Zr	Cellular Matrix: α-Al, Cell walls: α-Al_mFe, Particles: oval Al_6Fe, bar $Al_{13}Fe_4$	Cellular microstructure decomposition Matrix: α-Al Particles: needles $Al_{13}Fe_4$, globular Al_6Fe, bar $Al_{13}Fe_4$	Particles spheroidization and growth, Matrix: α-Al, Particles: globular and bar $Al_{13}Fe_4$, globular Al_3Zr, $Al_3Fe(Zr)$
Al-Fe-Zr-Si	Cellular, Matrix: α-Al, Cell walls: α-Al_mFe_nSi, Particles: $Al_xFe_ySi_z$	Cellular microstructure decomposition, Matrix: α-Al, Particles: Spherical $Al_xFe_ySi_z$	Particles spheroidization and growth, Matrix: α-Al, Particles: globular and spherical Al_3FeSi, Al_3Zr
Al-Fe-Zr-V	Cellular, Matrix: α-Al, Cell walls: α-Al_mFe, Particles: fine globular, $Al_mFe_n(V,Zr)$	Cellular microstructure decomposition, Matrix: α-Al, Particles: fine globular, $Al_xFe_y(V,Zr)$, globular and needles $Al_{13}Fe_4$	Particles spheroidization and growth, Matrix: α-Al, Particles: globular and bar $Al_{13}Fe_4$, spherical $Al_{10}V$, globular Al_3Zr

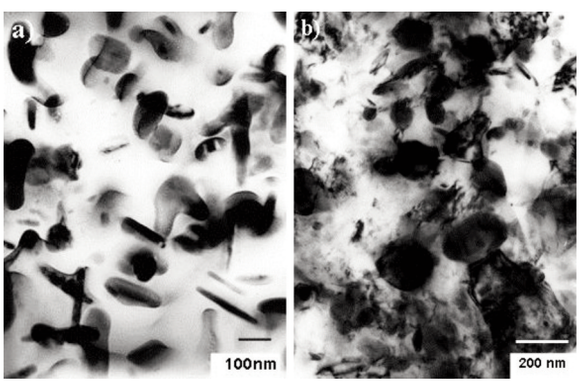

Figure 11. *a) Precipitation of $Al_{13}Fe_4$ during heating up to T_{m1}, b) decomposition of complex Al_xFe (V, Zr) phase into bar $Al_{13}Fe_4$ and globular $Al_{10}V$ particles*

Morphology of the particles interface doesn't indicate primary crystallization of this phase, but rather precipitation from supersaturated a_{Al} solid solution immediately after casting. The beginning of the decomposition of the cell microstructure coincides with the first temperature interval of variation in electrical resistance. The cell microstructure transformed into the globular and bar like particles of stable $Al_{13}Fe_4$ phase (Fig.11). Very seldom the needle shape particles were observed. Vanadium and zirconium were still detected in the a_{Al} solid solution as in the Al_xFe(V, Zr) fine globular particles. During heating up to temperature $T_{m2\text{-}AV,}$ metastable Al_xFe(V, Zr) phase transformed into stable $Al_{13}Fe_4$ and $Al_{10}V$ phases (Fig.11), with traces of zirconium. Zirconium also precipitated in the form of globular, 20¸50 nm large Al_3Zr phase particles.

4. Conclusions

All recordings of the electrical resistivity measurements during heating, show two distinctive temperature intervals where electrical resistivity changes in a non-linear way. From the microstructure of samples heated above T_{m1} can be seen, that decomposition of cell microstructure and precipitation of metastable and stable intermetalic phases from supersaturated a_{Al} solid solution occurred in the initial temperature interval. Precipitation phenomenon in this temperature interval is also confirmed with DSC and DTA measurements. Namely, the distinctive exothermal peak is detected at practically the same temperature as the first minima on the $^{dR}/_{dT}$ curve. The difference between T_{m1} and DSC and DTA exothermal peak temperature is only 1,5 °C for AS and 0,8 °C for AV alloy. From the comparison of the DSC, DTA and ER results can be concluded that the maximum precipitation rate is at T_{m1}. On the contrary, DSC and DTA measurements didn't detect heat release at a temperature interval where the second electrical resistivity change is detected, although microstructures of the samples heated above T_{m2} show complete transformation of metastable into stable intermetalic phases and precipitation of Al_3Zr phase. This inability of detection can be explained with the fact that transformations of the remaining metastable phases occur in a broad temperature interval and concur with the spheroidization and particle growth. Additionally, the weight fraction of the precipitated Al3Zr phase is very small. On the other hand, solute atoms are very effective scattering centers which increase electric resistivity of the matrix. Because all examined alloys have practically the same amount of added Zr, and maximum rate of the electrical resistivity decrease occurs at almost the same temperature (537±2°C), in our opinion, the electrical resistivity decrease in the second temperature interval can be ascribed to the precipitation of the Al_3Zr phase.

In as cast rapidly solidified Al-Fe-Zr-Si alloys, silicon can be found in Al_mFe_nSi complex eutectic

phases and a_{Al} solid solution. During heating above $T_{m1\text{-}AS}$ precipitates in the form of globular silicides and hinder the precipitation of acicular $Al_{13}Fe_4$ stable phase. Lower temperature of precipitation start could be a consequence of higher amount of alloying elements. During the heating above $T_{m2\text{-}AS}$, metastable silicides transform in to stable Al_3FeSi phase.

In as cast rapidly solidified Al-Fe-Zr-V alloys, vanadium can be found in aluminium matrix and complex Al_xFe_y(V,Zr) fine globular particles, stable above T_{m1}. During the heating above $T_{m2\text{-}AV}$ metastable Al_xFe_y (V, Zr) fine globular particles transform into stable $Al_{13}Fe_4$ and $Al_{10}V$ phases.

References

[1] Aluminium Handbook, Edited by C.Kammer, Aluminium Verlag, (1999)

[2] S.K.Das, F.H.Froes, in: H.H.Liebermann (Ed.), Rapidly Solidified Alloys, Marcel Dekker, (1993)

[3] V.I.Dobatkin et al in, N. A. Belov, A.A. Aksenov, D.G.Eskin: Iron in Aluminum Alloys, Taylor&Francis, (2002)

[4] M. Bizjak, L.. Kosec, A. C. Kneissl, B. Kosec., Int. Journal of Material Research, 1, (2008),101

[5] C.A.D. Rodrigues, D.R. Leiva, K.R. Cardoso, C.S. Kiminami, W.J.F. Botta., Materials Science Forum, 386-388, (2002), 33

[6] M. Bizjak, L. Kosec/, Zeitschrift fuer Metallkunde/Materials Research and Advanced Techniques, 91 (2), (2000) , 160

[7] C. Guo, Z. Du, C. Li, B. Zhang, M. Tao., Computer Coupling of Phase Diagrams and Thermochemistry, 32 (4),(2008), 637

[8] E. Karakose, M. Keskin., Materials and Design, 32, (2011), 4970

[9] L. Katgerman, F. Dom., Rapidly solidified alloys by meltspinning, 375 (2004) 1212

[10] H. Jones., Materials Letters, 26, (1996), 133

[11] S.K. Das, J.H. Perepezko, R.I. Wu, G. Wilde., Materials Science and Engineering, A304–306 (2001) 159

[12] B. Karpe, B. Kosec, T. Kolenko, M. Bizjak., Metalurgija, 50 (1) (2011) 13

[13] H. Matsumoto., Journal of Alloys and Compounds, 370 (2004) 244

[14] M.R. Corfield, I.R. Harris, A.J. Williams., Journal of Magnetism and Magnetic Materials, 316 (2007) 59

[15] D. Hamana, M. Bouchear, M. Betrouche, A. Derafa, N.Ya., Journal of Alloys and Compounds, 320 (2001) 93

[16] F. Prima, M. Tomuta, I. Stone, B. Cantor, D. Janickovic, G. Vlasak, P. Svec., Materials Science and Engineering, A 375–377 (2004) 772